crystals

MDPI

Article

Synthesis, Crystal Structure, Spectroscopic Properties, and DFT Studies of 7,9-Dibromobenzo[*h*]quinolin-10-ol

Hsing-Yang Tsai [1], Yuan Jay Chang [2], Jiun-Wei Hu [1] and Kew-Yu Chen [1,*]

[1] Department of Chemical Engineering, Feng Chia University, Taichung 40724, Taiwan; p0156676@fcu.edu.tw (H.-Y.T.); p0400205@fcu.edu.tw (J.-W.H.)

[2] Department of Chemistry, Tunghai University, Taichung 40704, Taiwan; jaychang@thu.edu.tw

* Correspondence: kyuchen@fcu.edu.tw; Tel.: +886-4-2451-7250 (ext. 3683); Fax: +886-4-2451-0890

Academic Editor: Roberto Centore

Received: 9 December 2016; Accepted: 18 February 2017; Published: 21 February 2017

Abstract: 7,9-Dibromobenzo[*h*]quinolin-10-ol (**1**), a benzo[*h*]quinolin-10-ol derivative, was synthesized and characterized by single-crystal X-ray diffraction. The crystal belongs to monoclinic space group $P2_1/n$, with a = 3.9573(4), b = 18.0416(18), c = 15.8210(16) Å, $\alpha = 90^\circ$, $\beta = 96.139(3)^\circ$, and $\gamma = 90^\circ$. Compound **1** exhibits an intramolecular six-membered-ring hydrogen bond, from which excited-state intramolecular proton transfer takes place, resulting in a proton-transfer tautomer emission of 625 nm in cyclohexane. The crystal structure is stabilized by intermolecular π–π interactions, which links a pair of molecules into a cyclic centrosymmetric dimer. Furthermore, the geometric structures, frontier molecular orbitals, and potential energy curves (PECs) for **1** in the ground and the first singlet excited state were fully rationalized by density functional theory (DFT) and time-dependent DFT calculations.

Keywords: 7,9-dibromobenzo[*h*]quinolin-10-ol; ESIPT; X-ray diffraction; DFT calculations

1. Introduction

The excited-state intramolecular proton transfer (ESIPT) reaction of benzo[*h*]quinolin-10-ol (**2**) and related derivatives has received much attention due to its fundamental importance and potential applications [1,2]. The ESIPT reaction usually involves the transfer of a hydroxyl proton to an imine nitrogen through an intramolecular hydrogen-bonding system [3–6]. The resulting proton-transfer tautomer (keto-form) exhibits considerable differences in molecular structure and electronic configuration from its corresponding ground state, i.e., a large Stokes shifted tautomer fluorescence. This unique optical property has found many diverse applications such as probes for solvation dynamics [7–9] and biological environments [10,11], fluorescence microscopy imaging [12], near-infrared fluorescent dyes [13], nonlinear optical materials [14], photochromic materials [15], chemosensors [16–20], and organic light-emitting diodes [21–26]. To expand the scope of **2**-based chromophores available for designing systems for laser dyes and fluorescent materials, the present research reports the synthesis of a benzo[*h*]quinolin-10-ol derivative 7,9-dibromobenzo[*h*]quinolin-10-ol (**1**) as well as its X-ray structure, spectroscopic properties, and complementary time-dependent density functional theory (TD-DFT) calculations. The results offer the potential for synthesizing benzo[*h*]quinolin-10-ol derivatives with extended molecular architectures and optical properties.

2. Results

Synthesis and Characterization

Scheme 1 depicts the synthetic route and the chemical structure of **1**. The bromination of **2** was carried out by the reaction of **2** with bromine in the presence of acetic acid, giving **1** in a good yield of 95% after purification. The structure of 7,9-dibromobenzo[*h*]quinolin-10-ol (**1**) can be verified by the presence of only seven signals (two singlet and two doublet signals and three doublet of doublets signals) at δ 7.0–17.0 ppm in the ^{1}H NMR spectrum, which indicates that the bromination at the 7,9-positions of **2** was achieved. To confirm its structure, a single crystal of **1** was obtained from a dichloromethane solution, and the molecular structure was determined by X-ray diffraction analysis. Moreover, its X-ray structure is compared with that of **2** [27].

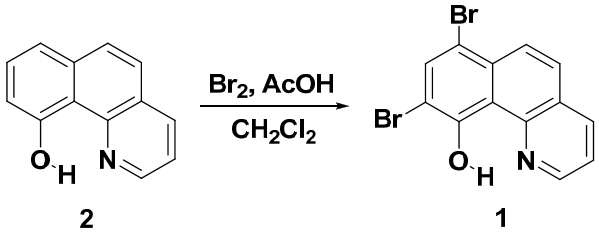

Scheme 1. The synthetic route and the structure for **1**.

3. Discussion

3.1. Hydrogen Bond Studies

The dominance of an enol-form for compounds **1** and **2** is supported by a combination of ^{1}H NMR and X-ray single-crystal analyses. In the ^{1}H NMR studies, the presence of a strong hydrogen bond between O–H and N is evidenced by the observation of a large downfield shift of the proton peak at δ > 14 ppm (in $CDCl_3$) for both compounds **1** (16.65 ppm) and **2** (14.86 ppm). According to Schaefer's equation [28], the hydrogen bonding energies (ΔE in kcal/mol) of **1** and **2** can be estimated to be as large as 12.8 ± 0.2 kcal/mol and 11.0 ± 0.2 kcal/mol, respectively. Note that the substitution of the hydrogen atoms at the 7,9-positions in **2** by bromine atoms, forming **1**, seems to increase the acidity of phenol (O–H) through an inductive effect. Thus, **1** exhibits a downfield shift of the O–H proton, and hence, a stronger hydrogen bond relative to **2**.

3.2. X-Ray Structures

Compound **1** crystallizes in the space group $P2_1/n$ with $Z' = 1$, whereas the closely related compound **2** crystallizes with $Z' = 2$ in the space group $Pbc2_1$ (Table 1). The *ORTEP* (Oak Ridge Thermal Ellipsoid Plot) diagram of **1** is shown in Figure 1. The complete molecule is almost planar, as indicated by the key torsion angles (Table 2). The maximum deviations from the mean plane through the non-H atoms are 0.025(1) Å for atom C(6) and 0.024(1) Å for atom O. The dihedral angle between the terminal ring planes is 0.9(2)°, which is slightly smaller than that in **2** (2.3(2)°). Compound **1** exhibits an intramolecular O–H···N hydrogen bond (green dashed line in Figure 1), which generates an S(6) ring motif [29–32]. The dihedral angle between the mean plane of the S(6) ring and the mean plane of the pyridine ring is 3.27(2)°. This, together with 2.529(8) Å of O···N distance and 144(8)° of O–H(0A)···N, strongly supports the six-membered-ring intramolecular hydrogen bonding formation. The parameters of the hydrogen bond of **1** (Table 3) are slightly different from those of **2** (2.562(5) Å of O(1)···N distance and 138(3)° of O(1)–H(0A)–N). Additionally, there is a weak intramolecular C–H···Br hydrogen bond in **1** (3.216(7) Å of C(6)···Br(2) distance and 109° of C(6)–H(6A)–Br(2), Table 3), which generates another S(5) motif. In good agreement with these observations, the ^{1}H NMR spectrum (in $CDCl_3$) revealed a significantly downfield signal at δ 8.14 ppm (H6A), giving a clear

indication of the five-membered ring intramolecular hydrogen bond formation. The bond-length and angle patterns of **1** are typical (Table S1); the long C(12)–C(13) bond (1.440(8) Å) and the short C(6)–C(7) bond (1.333(10) Å) support the results of the studies on *o*-phenanthroline [33].

Table 1. Crystallographic data for compounds **1** and **2**.

Compound	1	2
Chemical Formula	$C_{13}H_7Br_2NO$	$C_{13}H_9NO$
Formula Weight	353.02	195.21
Crystal System	Monoclinic	Orthorhombic
Space Group	$P2_1/n$	$Pbc2_1$
a (Å)	3.9573(4)	4.6530(4)
b (Å)	18.0416(18)	15.1910(10)
c (Å)	15.8210(16)	26.902(2)
α (°)	90	90
β (°)	96.139(3)	90
γ (°)	90	90
Volume (Å^3)	1123.1(2)	1901.5(2)
Z	4	8
D_{calc} (g cm^{-3})	2.088	1.364
μ (mm^{-1})	7.197	0.695
F_{000}	680	816
Crystal Size (mm^3)	0.38 × 0.08 × 0.07	0.35 × 0.20 × 0.15
θ range (°)	3.43–26.38	19.35–37.54
Index ranges	$-4 \leq h \leq 4$ $22 \leq k \leq 22$ $-19 \leq l \leq 19$	$0 \leq h \leq 5$ $0 \leq k \leq 16$ $0 \leq l \leq 29$
Reflections Collected	16148	1312
Independent Reflections (R_{int})	2266 (0.0438)	1312 (0.0000)
Refinement Method on F^2	Full-matrix least-squares	Full-matrix least-squares
GOF on F^2	1.095	1.213
R_1 [$I > 2\sigma(I)$]	0.0472	0.0383
wR_2 [$I > 2\sigma(I)$]	0.1296	0.0767
R_1 (All Data)	0.0729	0.0559
wR_2 (All Data)	0.1620	0.1128
Residual (e·Å^{-3})	1.100 and −0.507	0.117 and −0.131

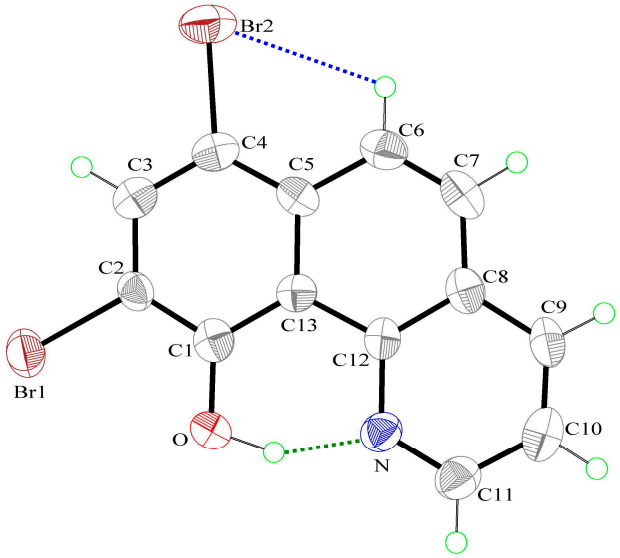

Figure 1. The molecular structure of **1**, showing the atom-labeling scheme. Displacement ellipsoids are drawn at the 50% probability level. Green and blue dashed lines denote the intramolecular O–H···N and C–H···Br hydrogen bonds.

Table 2. Comparison of the experimental and optimized geometric parameters of **1** (Å and °). DFT: Density Functional Theory.

Compound 1	X-ray	DFT
Bond Lengths (Å)		
O–C(1)	1.337(8)	1.361
N–C(11)	1.311(8)	1.342
N–C(12)	1.377(8)	1.380
C(2)–C(3)	1.386(9)	1.408
C(4)–C(5)	1.393(9)	1.421
C(6)–C(7)	1.333(10)	1.372
C(9)–C(10)	1.352(11)	1.396
C(12)–C(13)	1.440(8)	1.451
Br(1)–C(2)	1.892(6)	1.950
Br(2)–C(4)	1.901(6)	1.974
Bond Angles (°)		
C(11)–N–C(12)	120.0(5)	120.1
O–C(1)–C(2)	120.3(5)	120.2
C(1)–C(2)–C(3)	122.5(6)	121.2
C(4)–C(5)–C(6)	122.9(6)	123.2
C(9)–C(10)–C(11)	120.7(6)	118.6
C(8)–C(12)–C(13)	121.6(6)	120.7
Torsion Angles (°)		
C(12)–N–C(11)–C(10)	0.2(10)	0.1
O–C(1)–C(2)–Br(1)	–1.2(8)	–0.1
C(2)–C(3)–C(4)–C(5)	0.7(10)	0.1
C(6)–C(7)–C(8)–C(9)	179.5(7)	179.9
C(1)–C(13)–C(12)–C(8)	178.0(6)	179.9

Table 3. Hydrogen bond lengths (Å) and bond angles (°).

D–H···A	d(D–H)	d(H···A)	d(D···A)	∠DHA
O–H(0A)···N	1.00(9)	1.65(9)	2.529(8)	144(8)
C(6)–H(6A)···Br(2)	0.93	2.79	3.216(7)	109

The molecular packing of **1** in the crystal unit cell is shown in Figure 2. The crystal structure is stabilized by intermolecular π–π interactions, which links a pair of molecules into a cyclic centrosymmetric dimer. The pertinent measurements for these π···π interactions are centroid–centroid distances of 3.733(4) (black dashed lines, symmetry code: $1 + X, Y, Z$), 3.648(4) (pink dashed lines, symmetry code: $1 + X, Y, Z$), 3.734(4) (green dashed lines, symmetry code: $-1 + X, Y, Z$), and 3.648(4) Å (red dashed lines, symmetry code: $-1 + X, Y, Z$). These π···π interactions lead to the formation of dimers that are connected to another dimer via intermolecular Br(1)···Br(2) (3.5813(11) Å, blue dashed lines, symmetry code: $\frac{1}{2} + X, 3/2 - Y, \frac{1}{2} + Z$) contacts, so linking the molecules into a continuous three-dimensional framework.

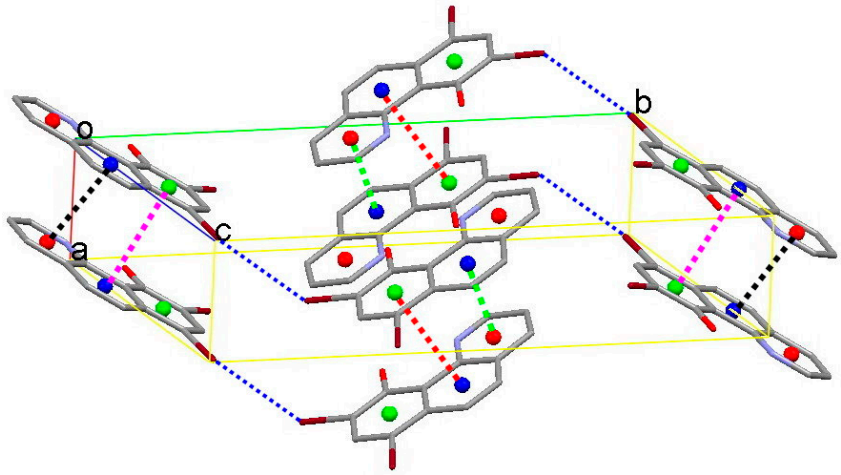

Figure 2. Part of the crystal structure in the unit cell of **1**, showing the formation of the dimmer built from π···π interactions. *Cg*1 (red circles), *Cg*2 (green circles), and *Cg*3 (blue circles) are the centroids of the C8–C12/N, C1–C5/C13, and C5–C8/C12/C13 rings, respectively. The black, pink, green, and red dashed lines denote different intermolecular π···π interactions. The blue dashed lines denote intermolecular Br(1)···Br(2) contacts. All hydrogen atoms are omitted for clarity.

3.3. Optical Properties

Figure 3 depicts the absorption and fluorescence spectra of **1** in cyclohexane. The longest wavelength absorption band of **1** appears at 376 nm, which is assigned to the π–π* transition (vide infra). Another higher energy absorption band is also observed at 314 nm. As for the steady-state emission, compound **1** exhibits a long wavelength emission at 625 nm in cyclohexane. Figure 3 also shows a large separation of the energy gap between the 0–0 onset of the absorption and emission. The Stokes shift of the emission, defined by the peak (absorption)-to-peak (emission) gap in terms of frequency, is calculated to be as large as 10,596 cm^{-1}. Accordingly, the assignment of 625 nm in cyclohexane to a proton-transfer tautomer emission is unambiguous [1,2], and ESIPT takes place from the phenolic proton to the pyridinic nitrogen, forming the keto-amine tautomeric species. This viewpoint can be further supported by a theoretical approach based on density functional theory (vide infra).

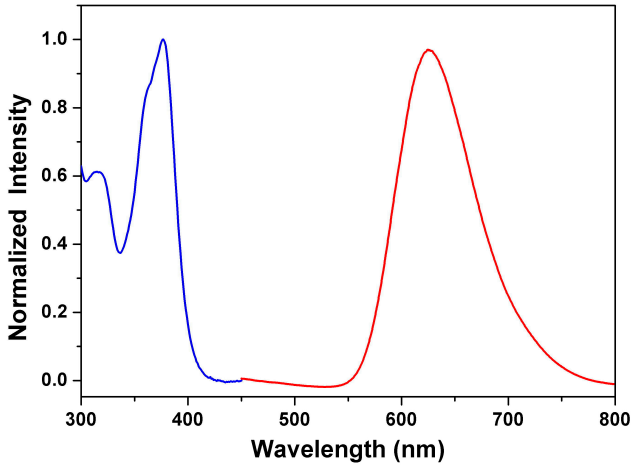

Figure 3. Normalized absorption (blue line) and emission (red line) spectra of **1** in cyclohexane.

3.4. Quantum Chemistry Computation

To gain more insight into the molecular structure and optical properties of **1**, quantum chemical calculations were performed using density functional theory (DFT) and time-dependent DFT (TD-DFT) at the B3LYP/LanL2DZ level. The geometric parameters were compared with the experimental data (Table 2). One can clearly see that there are no significant differences between the experimental and DFT/B3LYP calculated geometric parameters. Therefore, we can conclude that basis set LanL2DZ is suited in its approach to the experimental results.

Figure 4 depicts the optimized geometric structures (Table S2) and the corresponding hydrogen bond lengths of the enol form for **1** and **2** in the ground (S_0) and the first singlet excited state (S_1). From E to E*, we can see that the intramolecular hydrogen bond length (red dashed lines) decreases from 1.58 (1.77) Å to 1.46 (1.66) Å for **1** (**2**). The results distinctly provide the evidence for the strengthening of the intramolecular hydrogen bond from $S_0 \rightarrow S_1$. Consequently, there is no doubt that the decrease of the intramolecular hydrogen bond lengths from E to E* is a very important positive factor for the ESIPT reaction.

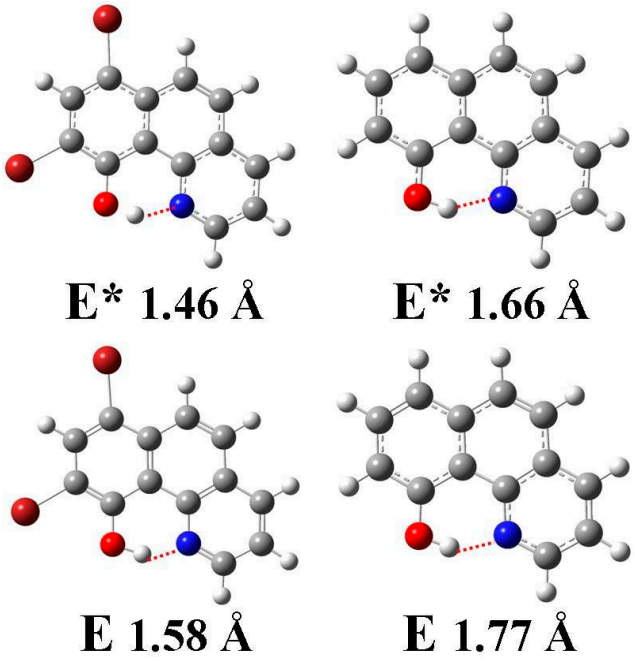

Figure 4. The optimized geometric structures of the enol (E) form for **1** (left) and **2** (right) in the ground (S_0) and the first singlet excited state (S_1) together with the intramolecular hydrogen bond lengths. The red dashed lines denote the intromolecular O–H$\cdots$N hydrogen bonds.

The highest occupied molecular orbitals (HOMOs) and the lowest unoccupied molecular orbitals (LUMOs) of the enol and keto forms of **1** are shown in Figure 5. The first excited states for both the normal (enol) and tautomer (keto) forms are a dominant $\pi \rightarrow \pi^*$ transition from the HOMO to the LUMO. Figure 5 also shows that the electron density around the intramolecular hydrogen bonding system is mainly populated with hydroxyl oxygen and pyridinic nitrogen in the HOMO and LUMO, respectively. The results clearly indicate that, upon electronic excitation of **1**, the hydroxyl proton (O–H) is expected to be more acidic, whereas the pyridinic nitrogen is more basic with respect to its ground state, driving the excited-state intramolecular proton transfer reaction. Moreover, the absorption and fluorescence spectra of **1** were calculated by time-dependent DFT calculations (Franck–Condon principle). The calculated excitation (emission) wavelength for the $S_0 \rightarrow S_1$ ($S_1 \rightarrow S_0$) transition is 392 (631) nm, which is slightly higher but in good agreement with experimental results.

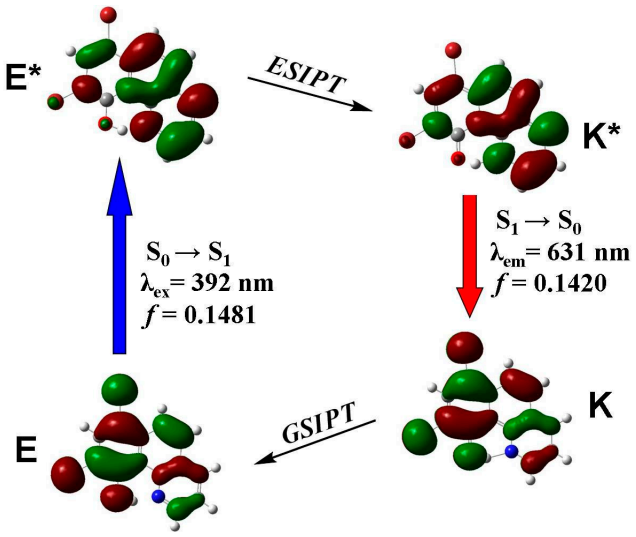

Figure 5. Selected frontier molecular orbitals involved in the excitation and emission of **1**.

In an effort to explain the ESIPT reaction of **1**, the potential energy curves (PECs) of the intramolecular proton transfer at both the ground state and the excited state were scanned, keeping the O–H bond lengths fixed at values in the range from 1.03 Å to 1.83 Å in steps of 0.1 Å, as shown in Figure 6. The energy of the S_0 state increases along with the lengthening of the O–H bond and the potential barrier is 4.8 kcal/mol. The potential energy curve of the S_1 state indicates that the ESIPT reaction is a barrierless process and the tautomeric structure of the reaction product is the only minimum on the excited state surface. The results clearly show that the ESIPT for **1** is thermodynamically favorable, which is consistent with the experimental results.

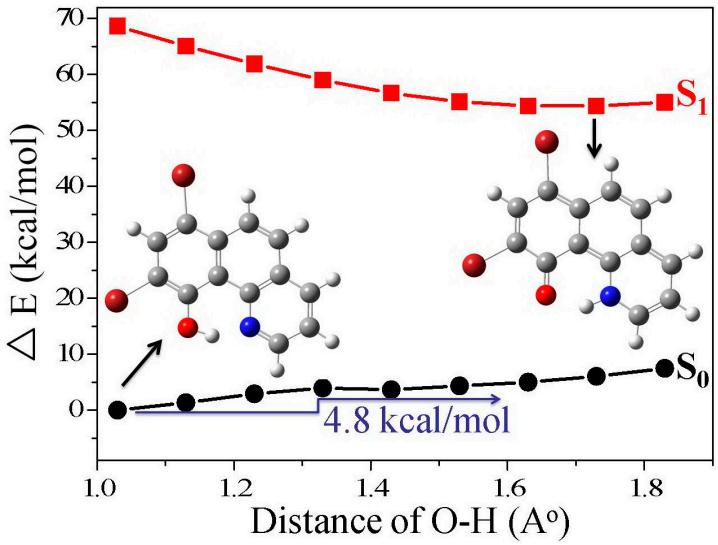

Figure 6. Potential energy curves of S_0 and S_1 states for **1** along with the O–H bond length. The insert shows the corresponding optimized geometries.

4. Materials and Methods

4.1. Chemicals and Instruments

The starting materials such as benzo[*h*]quinolin-10-ol (**2**), bromine, acetic acid, and dichloromethane were purchased from Merck (Whitehouse Station, NJ, USA), ACROS (Pittsburgh, PA,

USA), and Sigma–Aldrich (St. Louis, MO, USA). Column chromatography was performed using silica gel Merck Kieselgel *si* 60 (40–63 mesh).

^{1}H NMR spectra were recorded in $CDCl_3$ on a Bruker 400 MHz. Mass spectra were recorded on a VG70-250S mass spectrometer (Hitachi, Tokyo, Japan). The absorption and emission spectra were measured using a Jasco V-570 UV–Vis spectrophotometer (Jasco, Tokyo, Japan) and a Hitachi F-4500 fluorescence spectrophotometer (Hitachi, Tokyo, Japan), respectively. The single-crystal X-ray diffraction data were collected on a Bruker Smart 1000CCD area-detector diffractometer (Bruker, Billerica, MA, USA).

4.2. Synthesis and Characterization

A solution containing benzo[*h*]quinolin-10-ol (195 mg, 1.0 mmol) and acetic acid (1.0 mL) in dichloromethane (30 mL) were added to a solution of bromine (960 mg, 2.7 mmol) for a period of 1 h. The reaction mixture was refluxed for 2 h. After cooling, the mixture was neutralized with 10% KOH and extracted with CH_2Cl_2 (3 × 30 mL). After the solvent was removed, the crude product was purified by silica gel column chromatography with eluent ethyl acetate/*n*-hexane (1/4) to afford **1** (353 mg, 95%). ^{1}H NMR (400 MHz, $CDCl_3$, in ppm) δ 16.65 (s, 1H, H_7), 8.90 (dd, J_1 = 4.6 Hz, J_2 = 1.6 Hz, H_1), 8.60 (s, H_6), 8.37 (dd, J_1 = 8.1 Hz, J_2 = 1.6 Hz, H_3), 8.14 (d, J = 9.2 Hz, H_5), 7.81 (d, J = 9.2 Hz, H_4), 7.71 (dd, J_1 = 8.1 Hz, J_2 = 4.6 Hz, H_2); Mass (EI, 70eV); m/z (relative intensity) 352 (M^+, 100); and high-resolution mass (HRMS) were calculated for $C_{13}H_7Br_2NO$ 352.8874 and found to be 352.8880. Red parallelepiped-shaped crystals suitable for the crystallographic studies reported here were isolated over a period of four weeks by slow evaporation from a dichloromethane solution.

4.3. Crystal Structural Determination

A single crystal of the title compound with dimensions of 0.38 mm × 0.08 mm × 0.07 mm was selected. The lattice constants and diffraction intensities were measured with a Bruker Smart 1000CCD area detector (Bruker, Billerica MA, USA) radiation (λ = 0.71073 Å) at 302(2) K. An ω-2θ scan mode was used for data collection in the range of $3.437 \leq \theta \leq 26.378^\circ$. A total of 16148 reflections were collected and 2266 were independent (R_{int} = 0.0438), of which 1679 were considered to be observed with $I > 2\sigma(I)$ and used in the succeeding refinement. The structure was solved by direct methods with SHELXS-97 [34] and refined on F^2 by a full-matrix least-squares procedure with Bruker SHELXL-97 packing [35]. All non-hydrogen atoms were refined with anisotropic thermal parameters. The hydrogen atoms, refined isotropically with riding model position parameters, were located from a difference Fourier map and added theoretically. At the final cycle of refinement, R = 0.0472 and wR = 0.1296 ($w = 1/[\sigma^2(F_o^2) + (0.0856P)^2 + 3.9902P]$, where $P = (F_o^2 + 2F_c^2)/3$). S = 1.095, $(\Delta/\sigma)_{max}$ = 0.007, $(\Delta/\varrho)_{max}$ = 3.932 and $(\Delta/\varrho)_{min} = -1.923$ e/ Å^3, were observed. Crystallographic data for the structure reported in this article have been deposited in the Cambridge Crystallographic Data Center with a supplementary publication number of CCDC 1486418. Copies of this information can be obtained free of charge from the Director, CCDC, 12 Union Road, Cambridge CB2 1EZ, UK (Fax: +44-1223-336-033; e-mail: deposit@ccdc.cam.ac.uk).

4.4. Computational Methods

In the present work, all theoretical calculations were carried out using the Gaussian 03 program suite [36]. The electronic geometric optimizations of the enol and keto forms for **1** in the ground (S_0), and the first singlet excited state (S_1) was performed using density functional theory (DFT) and time-dependent DFT (TD-DFT) methods with the LanL2DZ basis set and the B3LYP functional. There were no constraints to all the atoms, bonds, angles, and dihedral angles during the geometric optimization. The vibrational frequencies were calculated using the same method to verify that the optimized structures correspond to the local minima on the energy surface. After obtaining the converged geometries, the TD-B3LYP/LanL2DZ was used to calculate the vertical excitation energy, and the tautomer emission energy was obtained from TD-DFT/B3LYP/LanL2DZ calculations

performed on the S_1 optimized geometry. As observed by the only slightly solvent polarity dependent shift of the emission (absorption) spectra in **1**, the charge transfer character of tautomer emission for **1** is slim. Thus, solvent effects are not considered throughout these computations [37]. In addition to the unconstrained optimization, constrained calculations on the S_0 and S_1 potential energy curves of **1** were scanned, keeping the O−H bond lengths fixed at values in the range from 1.03 Å to 1.83 Å in steps of 0.1 Å. The energies shown in the curves are relative values, with the lowest point on the curve as zero.

5. Conclusions

A benzo[*h*]quinolin-10-ol derivative, namely, 7,9-dibromobenzo[*h*]quinolin-10-ol (**1**) was synthesized and fully characterized. Compound **1** exhibits an intramolecular six-membered-ring hydrogen bond, from which ESIPT takes place, resulting in a proton-transfer tautomer emission of 625 nm in cyclohexane. The geometric structures, frontier molecular orbitals, and potential energy curves (PECs) for **1** in the ground and the first singlet excited state were fully rationalized by DFT and time-dependent DFT calculations and were in good agreement with the experimental results. In addition, the single-crystal X-ray structure determinations reported here have brought to light many interesting properties between **1** and **2** in the solid state, including intra- and intermolecular hydrogen bonding interactions and $\pi\cdots\pi$ stacking. This offers the potential to synthesize benzo[*h*]quinolin-10-ol derivatives with extended molecular architectures and optical properties.

Supplementary Materials: The following are available online at www.mdpi.com/2073-4352/7/2/60/s1; Table S1: Bond lengths and angles for **1**. Table S2: Total and relative energies of **1** and **2** in the ground state.

Acknowledgments: The project was supported by the Ministry of Science and Technology (MOST 105-2113-M-035-001). The authors appreciate the Precision Instrument Support Center of Feng Chia University for providing the fabrication and measurement facilities.

Author Contributions: Hsing-Yang Tsai synthesized the compound. Jiun-Wei Hu measured the data. Yuan Jay Chang and Kew-Yu Chen prepared the manuscript.

Conflicts of Interest: The authors declare no conflict of interest.

References

1. Chou, P.T.; Wei, C.Y. Photophysics of 10-hydroxybenzo[h]quinoline in aqueous solution. *J. Phys. Chem.* **1996**, *100*, 17059–17066. [CrossRef]
2. Chen, K.Y.; Hsieh, C.C.; Cheng, Y.M.; Lai, C.H.; Chou, P.T. Extensive spectral tuning of the proton transfer emission from 550 to 675 nm *via* a rational derivatization of 10-hydroxybenzo[*h*]quinoline. *Chem. Commun.* **2006**, *42*, 4395–4397. [CrossRef] [PubMed]
3. Satam, M.A.; Raut, R.K.; Telore, R.D.; Sekar, N. Fluorescent acid azo dyes from 3-(1,3-benzothiazol-2-yl)naphthalen-2-ol and comparison with 2-naphthol analogs. *Dyes Pigment.* **2013**, *97*, 32–42. [CrossRef]
4. Luo, M.H.; Tsai, H.Y.; Lin, H.Y.; Fang, S.K.; Chen, K.Y. Extensive spectral tuning of the proton transfer emission from green to red via a rational derivatization of salicylideneaniline. *Chin. Chem. Lett.* **2012**, *23*, 1279–1282. [CrossRef]
5. Fang, T.C.; Tsai, H.Y.; Luo, M.H.; Chang, C.W.; Chen, K.Y. Excited-state charge coupled proton transfer reaction via the dipolar functionality of salicylideneaniline. *Chin. Chem. Lett.* **2013**, *24*, 145–148. [CrossRef]
6. Satam, M.A.; Raut, R.K.; Sekar, N. Fluorescent azo disperse dyes from 3-(1,3-benzothiazol-2-yl)naphthalen-2-ol and comparison with 2-naphthol analogs. *Dyes Pigment.* **2013**, *96*, 92–103. [CrossRef]
7. Chen, K.Y.; Tsai, H.Y. Synthesis, X-ray structure, spectroscopic properties and DFT studies of a novel Schiff base. *Int. J. Mol. Sci.* **2014**, *15*, 18706–18724. [CrossRef] [PubMed]
8. Xie, L.; Chen, Y.; Wu, W.; Guo, H.; Zhao, J.; Yu, X. Fluorescent coumarin derivatives with large stokes shift, dual emission and solid state luminescent properties: An experimental and theoretical study. *Dyes Pigment.* **2012**, *92*, 1361–1369. [CrossRef]
9. Mahapatra, A.K.; Maiti, K.; Sahoo, P.; Nandi, P.K. A new colorimetric and fluorescent bis(coumarin)methylene probe for fluoride ion detection based on the proton transfer signaling mode. *J. Lumin.* **2013**, *143*, 349–354. [CrossRef]

10. Lim, C.K.; Seo, J.; Kim, S.; Kwon, I.C.; Ahn, C.H.; Park, S.Y. Concentration and pH-modulated dual fluorescence in self-assembled nanoparticles of phototautomerizable biopolymeric amphiphile. *Dyes Pigment.* **2011**, *90*, 284–289. [CrossRef]
11. Hong, W.H.; Lin, C.C.; Hsieh, T.S.; Chang, C.C. Preparation of fluoroionophores based on diamine-salicylaldehyde derivatives. *Dyes Pigment.* **2012**, *94*, 371–379. [CrossRef]
12. Chen, K.Y.; Cheng, Y.M.; Lai, C.H.; Hsu, C.C.; Ho, M.L.; Lee, G.H.; Chou, P.T. Ortho green fluorescence protein synthetic chromophore; excited-state intramolecular proton transfer via a seven-membered-ring hydrogen-bonding system. *J. Am. Chem. Soc.* **2007**, *129*, 4534–4535. [CrossRef] [PubMed]
13. Zhang, M.; Yang, D.; Ren, B.; Wang, D. A TDDFT study on the excited-state intramolecular proton transfer (ESIPT): Excited-state equilibrium induced by electron density swing. *J. Fluoresc.* **2013**, *23*, 761–766. [CrossRef] [PubMed]
14. Ashraf, M.; Teshome, A.; Kay, A.J.; Gainsford, G.J.; Bhuiyan, M.D.H.; Asselberghs, I.; Clays, K. Synthesis and optical properties of NLO chromophores containing an indoline donor and azo linker. *Dyes Pigment.* **2012**, *95*, 455–464. [CrossRef]
15. Lin, W.C.; Fang, S.K.; Hu, J.W.; Tsai, H.Y.; Chen, K.Y. Ratiometric fluorescent/colorimetric cyanide-selective sensor based on excited-state intramolecular charge transfer-excited-state intramolecular proton transfer switching. *Anal. Chem.* **2014**, *86*, 4648–4652. [CrossRef] [PubMed]
16. Zhang, Y.J.; He, X.P.; Hu, M.; Li, Z.; Shi, X.X.; Chen, G.R. Highly optically selective and electrochemically active chemosensor for copper (II) based on triazole-linked glucosyl anthraquinone. *Dyes Pigment.* **2011**, *88*, 391–395. [CrossRef]
17. Huang, Q.; Yang, X.F.; Li, H. A ratiometric fluorescent probe for hydrogen sulfide based on an excited-state intramolecular proton transfer mechanism. *Dyes Pigm.* **2013**, *99*, 871–877. [CrossRef]
18. Prabhu, S.; Saravanamoorthy, S.; Ashok, M.; Velmathi, S. Colorimetric and fluorescent sensing of multi metal ions and anions by salicylaldimine based receptors. *J. Lumin.* **2012**, *132*, 979–986. [CrossRef]
19. Patil, V.S.; Padalkar, V.S.; Tathe, A.B.; Sekar, N. ESIPT-inspired benzothiazole fluorescein: Photophysics of microenvironment pH and viscosity. *Dyes Pigment.* **2013**, *98*, 507–517. [CrossRef]
20. Ito, Y.; Amimoto, K.; Kawato, T. Prototropic tautomerism and solid-state photochromism of *N*-phenyl-2-aminotropones. *Dyes Pigment.* **2011**, *89*, 319–323. [CrossRef]
21. Li, Y.; Wang, D.; Wang, L.; Li, Z.; Cui, Q.; Zhang, H.; Yang, H. Novel asymmetrical pyrene derivatives as light emitting materials: Synthesis and photophysics. *J. Lumin.* **2012**, *132*, 1010–1014. [CrossRef]
22. Chuang, W.T.; Hsieh, C.C.; Lai, C.H.; Lai, C.H.; Shih, C.W.; Chen, K.Y.; Hung, W.Y.; Hsu, Y.H.; Chou, P.T. Excited-state intramolecular proton transfer molecules bearing *o*-hydroxy analogues of green fluorescent protein chromophore. *J. Org. Chem.* **2011**, *76*, 8189–8202. [CrossRef] [PubMed]
23. Xu, H.; Yue, Y.; Wang, H.; Chen, I.; Hao, Y.; Xu, B. Single-crystal structure, photophysical characteristics and electroluminescent properties of bis(2-(4-trifluoromethyl-2-hydroxyphenyl)benzothiazolate)zinc. *J. Lumin.* **2012**, *132*, 919–923. [CrossRef]
24. Tang, K.C.; Chang, M.J.; Lin, T.Y.; Pan, H.A.; Fang, T.C.; Chen, K.Y.; Hung, W.Y.; Hsu, Y.H.; Chou, P.T. Fine tuning the energetics of excited-state intramolecular proton transfer (ESIPT): White light generation in a single ESIPT system. *J. Am. Chem. Soc.* **2011**, *133*, 17738–17745. [CrossRef] [PubMed]
25. Fang, S.K.; Tsai, H.Y.; Hu, J.W.; Chen, K.Y. A white-light-emitting small molecule: Synthesis, crystal structure and optical properties. *Int. J. Photoenergy* **2014**. [CrossRef]
26. Hu, J.W.; Wu, Y.H.; Tsai, H.Y.; Chen, K.Y. Synthesis, X-ray structure, optical, and electrochemical properties of a white-light-emitting molecule. *Materials* **2016**, *9*, 48. [CrossRef]
27. Kubicki, M.; Borowiak, T.; Antkowiak, W.Z. 10-Hydroxybenzo[h]quinoline. *Acta Cryst.* **1995**, *C51*, 1173–1175. [CrossRef]
28. Schaefer, T. Relation between hydroxyl proton chemical shifts and torsional frequencies in some ortho-substituted phenol derivatives. *J. Phys. Chem.* **1975**, *79*, 1888–1890. [CrossRef]
29. Chen, K.Y.; Hu, J.W. Excited-state charge coupled proton transfer reaction in dipole-functionalized salicylideneaniline. *J. Lumin.* **2015**, *159*, 171–177. [CrossRef]
30. Chen, K.Y. Crystal structure, hydrogen-bonding properties and DFT studies of 2-((2-(2-hydroxyphenyl)benzo[*d*]thiazol-6-yl)methylene)malononitrile. *Mol. Cryst. Liq. Cryst.* **2015**, *623*, 285–296. [CrossRef]

31. Chen, K.Y.; Tsai, H.Y.; Lin, W.C.; Chu, H.H.; Weng, Y.C.; Chan, C.C. ESIPT fluorescent dyes with adjustable optical properties: Substituent and conjugation effects. *J. Lumin.* **2014**, *154*, 168–177. [CrossRef]
32. Chen, K.Y.; Tsai, H.Y.; Lin, W.C.; Chu, H.H.; Weng, Y.C.; Chan, C.C. Synthesis, crystal structure, optical and electrochemical properties of 9,10-dihydroxybenzo[*h*]quinoline. *J. Chem. Sci.* **2014**, *124*, 955–966. [CrossRef]
33. Nishigaki, S.; Yoshioka, H.; Nakatsu, K. The crystal and molecular structure of o-phenanthroline. *Acta Cryst.* **1978**, *B34*, 875–879. [CrossRef]
34. Sheldrick, G.M. *SHELXS97, A Program for Automatic Solution of Crystal Structure*; University of Göttingen: Göttingen, Germany, 1997.
35. Sheldrick, G.M. *SHELX97, A Program for Crystal Structure Refinement*; University of Göttingen: Göttingen, Germany, 1997.
36. Frisch, M.J.; Trucks, G.W.; Schlegel, H.B.; Scuseria, G.E.; Robb, M.A.; Cheeseman, J.R.; Montgomery, J.A.; Vreven, T., Jr.; Kudin, K.N.; Burant, J.C.; et al. *Gaussian 03*; Gaussian, Inc.: Pittsburgh, PA, USA, 2003.
37. Capobianco, A.; Borrelli, R.; Landi, A.; Velardo, A.; Peluso, A. Absorption band shapes of a push–pull dye approaching the cyanine limit: A challenging case for first principle calculations. *J. Phys. Chem. A* **2016**, *120*, 5581–5589. [CrossRef] [PubMed]